NASA/TM–2016-219188
NESC-RP-13-00860

Carbon Fiber Strand Tensile Failure Dynamic Event Characterization

Kenneth L. Johnson/NESC
Langley Research Center, Hampton, Virginia

James Reeder
Langley Research Center, Hampton, Virginia

April 2016

NASA STI Program . . . in Profile

Since its founding, NASA has been dedicated to the advancement of aeronautics and space science. The NASA scientific and technical information (STI) program plays a key part in helping NASA maintain this important role.

The NASA STI program operates under the auspices of the Agency Chief Information Officer. It collects, organizes, provides for archiving, and disseminates NASA's STI. The NASA STI program provides access to the NTRS Registered and its public interface, the NASA Technical Reports Server, thus providing one of the largest collections of aeronautical and space science STI in the world. Results are published in both non-NASA channels and by NASA in the NASA STI Report Series, which includes the following report types:

- TECHNICAL PUBLICATION. Reports of completed research or a major significant phase of research that present the results of NASA Programs and include extensive data or theoretical analysis. Includes compilations of significant scientific and technical data and information deemed to be of continuing reference value. NASA counter-part of peer-reviewed formal professional papers but has less stringent limitations on manuscript length and extent of graphic presentations.
- TECHNICAL MEMORANDUM. Scientific and technical findings that are preliminary or of specialized interest, e.g., quick release reports, working papers, and bibliographies that contain minimal annotation. Does not contain extensive analysis.
- CONTRACTOR REPORT. Scientific and technical findings by NASA-sponsored contractors and grantees.
- CONFERENCE PUBLICATION. Collected papers from scientific and technical conferences, symposia, seminars, or other meetings sponsored or co-sponsored by NASA.
- SPECIAL PUBLICATION. Scientific, technical, or historical information from NASA programs, projects, and missions, often concerned with subjects having substantial public interest.
- TECHNICAL TRANSLATION. English-language translations of foreign scientific and technical material pertinent to NASA's mission.

Specialized services also include organizing and publishing research results, distributing specialized research announcements and feeds, providing information desk and personal search support, and enabling data exchange services.

For more information about the NASA STI program, see the following:

- Access the NASA STI program home page at *http://www.sti.nasa.gov*
- E-mail your question to help@sti.nasa.gov
- Phone the NASA STI Information Desk at 757-864-9658
- Write to:
  NASA STI Information Desk
  Mail Stop 148
  NASA Langley Research Center
  Hampton, VA 23681-2199

NASA/TM–2016-219188
NESC-RP-13-00860

Carbon Fiber Strand Tensile Failure Dynamic Event Characterization

Kenneth L. Johnson/NESC
Langley Research Center, Hampton, Virginia

James Reeder
Langley Research Center, Hampton, Virginia

National Aeronautics and
Space Administration

Langley Research Center
Hampton, Virginia 23681-2199

April 2016

Acknowledgments

The authors wish to recognize Dr. Donald Shockey, SRI International, Menlo Park, California for his questions regarding carbon composite fiber failure modes that helped found and guide this task, and the LaRC materials lab staff and management who provided the facility and expertise needed for its successful performance. Mr. Jonny Callahan at LaRC (Science and Technology Corporation) installed test rig interface grips to strand articles supplied by the MSFC Structural Materials team headed by Mr. W. Chad Hastings. Mr. Callahan also operated the tensile strength test equipment at LaRC. None of this work would have been possible without their efforts. We also appreciate Dr. Pappu L. N. Murthy of NASA Glenn Research Center and Drs. William Prosser and Robert Piascik of the NESC (both located at LaRC) for their support and guidance.

Available from:

NASA STI Program / Mail Stop 148
NASA Langley Research Center
Hampton, VA 23681-2199
Fax: 757-864-6500

Carbon Fiber Strand Tensile Failure Dynamic Event Characterization

February 25, 2016

The information package containing the videos, presentations, papers, etc. mentioned in this paper will be made available on the NASA Engineering Network (NEN) Materials Community of Practice website (https://nen.nasa.gov/web/materials/documents) and possibly other sites.

Report Approval and Revision History

NOTE: This document was approved at the February 25, 2016, NRB. This document was submitted to the NESC Director on April 11, 2016, for configuration control.

Approved:	*Original Signature on File*	4/12/16
	NESC Director	Date

Version	Description of Revision	Office of Primary Responsibility	Effective Date
1.0	Initial Release	Mr. Kenneth L. Johnson, NESC Integration Office (NIO), MSFC	02/25/2016

Table of Contents

List of Figures

List of Tables

Technical Assessment Report

1.0 Notification and Authorization

Leads and members of the Composite Pressure Vessel Working Group (CPVWG) and of NASA Engineering and Safety Center (NESC) assessment TI-13-00912 Composite Overwrapped Pressure Vessel (COPV) Stress Rupture Reliability (13-00912) requested visual and other primary engineering physics data regarding failure modes in carbon fiber strands relevant to composite pressure vessel reliability. At the time this investigation was begun, the 13-00912 team was developing methods for interfacing new-design carbon fiber strand test articles with a new-design strand test rig. A candidate test article-to-test rig interface (grip) was being tested at Langley Research Center (LaRC). The LaRC Fatigue and Fracture Lab had both the expertise and equipment to begin to develop and perform some measurements and methods that could be used to answer basic engineering questions posed for minimum additional cost.

Dr. James Reeder of LaRC, member of the CPVWG and a principal investigator (PI) on the 13-00912 task, submitted a request to the NESC in March 2013. The NESC approved the request on March 14, 2013, as a priority 2 (Safety or Technical Assessment in support of Projects in the Design Phase) due to its impact on design development of the grips critical to success of the 13-00912 task. The 13-00912 task in turn has impact on risk assessment of existing International Space Station and other COPVs in use and in development. The task's deliverables are expected to have broad applicability in understanding of the physics of failure in an important and growing class of pressure vessels at NASA, in defense, in civilian transport, and many other applications. Mr. Kenneth L. Johnson, NESC representative located at Marshall Space Flight Center (MSFC), was assigned as the NESC lead. Dr. James Reeder was assigned as PI.

Key stakeholders for this task are CPVWG and 13-00912 assessment lead Dr. Lorie Grimes-Ledesma, Dr. Reeder, and other members of the CPVWG.

2.0 Signature Page

Submitted by:

Team Signature Page on Final – 4/13/2016

____

Mr. Kenneth L. Johnson   Date

Significant Contributors:

____

Dr. James Reeder   Date

Signatories declare the findings, observations, and NESC recommendations compiled in the report are factually based from data extracted from program/project documents, contractor reports, and open literature, and/or generated from independently conducted tests, analyses, and inspections.

3.0 Team List

Name	Discipline	Organization
Core Team		
Kenneth L. Johnson	NESC Lead	MSFC
James Reeder	Materials (Principal Investigator)	LaRC
Linda Anderson	MTSO Program Analyst	LaRC
Consultants		
Michael W. Czabaj	Materials Imaging/X-Ray Tomography	LaRC
David S. Dawicke	Materials Imaging/High-Speed and Digital Image Correlation	LaRC/AMA
Lorie Grimes-Ledesma	Composite Pressure Vessels	JPL
Joseph Zalameda	Materials Imaging/ Thermography	LaRC
Administrative Support		
Dee Bullock	Technical Writer	LaRC/AMA

3.1 Acknowledgements

The authors wish to recognize Dr. Donald Shockey, SRI International, Menlo Park, California for his questions regarding carbon composite fiber failure modes that helped found and guide this task, and the LaRC materials lab staff and management who provided the facility and expertise needed for its successful performance. Mr. Jonny Callahan at LaRC (Science and Technology Corporation) installed test rig interface grips to strand articles supplied by the MSFC Structural Materials team headed by Mr. W. Chad Hastings. Mr. Callahan also operated the tensile strength test equipment at LaRC. None of this work would have been possible without their efforts. We also appreciate Dr. Pappu L. N. Murthy of NASA Glenn Research Center and Drs. William Prosser and Robert Piascik of the NESC (both located at LaRC) for their support and guidance.

4.0 Executive Summary

There does not appear to be a good visual image record of carbon fiber strands failing. Failures occur over a very short time frame, much faster than visible with standard photography. Strand coupons used in testing are small and uniformly black. It is a dynamic event, but changes in the strand leading to failure are small, subtle, and at least in part unknown. Failure produces a destructive shock in the remaining material, turning much of it to dust and making post-mortem analysis impossible.

All of this makes it difficult to discuss the physics of failure with authority. An alternate viewpoint[1], referenced in NASA/TM-2012-217564 (Composite Pressure Vessel Working Group Task 3: Stress Rupture Test Approach), expressed this fact, noting, "Tests should be devised and performed to identify and measure the evolution of damage in composite overwrapped pressure vessel strands and walls with time and stress."

This task was an initial attempt to identify and measure that progression of damage leading to failure of a carbon fiber strand. It was not aimed at solving all problems; rather, it was to allow researchers to visualize what failures look like, at least on a gross scale, and allow the next questions to be asked. This main goal was achieved.

Test articles were 26 cylindrical strands made of polyacrylonitrile-based intermediate modulus carbon fiber (designated T1000GB) manufactured by Toray. The composite matrix is undiluted clear difunctional bisphenol A/epichlorohydrin-derived liquid epoxy manufactured by Momentive Specialty Chemicals designated as EPON 828 and cross-linked with a curing agent designated as EPIKURE™ Curing Agent W. The strands were imaged while under increasing tensile load applied longitudinally. Most were loaded to failure. Several imaging techniques, mainly high-speed video but also digital image correlation, thermography, and X-ray computed tomography (CT) scanning, were ultimately used to examine the strands as and after they were pulled to failure. These were tried to learn directly about strand failure and to give future researchers baseline information on useful measurement and evaluation methods. Each was found to give useful information, but all require development before being readily leveraged as effective tools in this application.

It was found that strands might fail in tension in several scenarios. Some appear to experience an essentially single catastrophic transverse break while others demonstrate a sequence of failures of groups of fibers. Some strands shatter longitudinally, producing fine slivers, while other strands break into large segments with comparatively few longitudinal breaks. There is evidence from X-ray CT that individual fibers are ruptured during loading, though this needs further study.

---

[1] If a consensus cannot be reached within the team or with an NESC Review Board member on one or more technical aspects of the report, then the specific areas of concern are documented as an alternative viewpoint. Disputed views by the Program/Project/Organization, or any other interested individual are not included.

In this case, the team reported that the best path forward was to estimate reliability of carbon fiber strands and vessels due to stress rupture failure modes empirically. The alternative viewpoint was that investigation into the physics of failure could be a more direct route.

Information useful to the 13-00912 task was also obtained. This information led to improvements in grip design, techniques for discerning between failure modes, and inputs into analysis methods planning.

Eight findings and one observation were identified in this investigation (Section 8.0). No NESC Recommendations are contained in this report.

Also associated with this report is an information package including exemplar imagery taken during task performance, particularly many high-speed videos of strands showing strand failure in lengthwise tension. Limited qualitative data associated with strength testing are supplied as well. Additional attachments outline lessons learned in setting up and performing imaging.

The information package containing the videos, presentations, papers, etc. mentioned in this paper will be made available on the NASA Engineering Network (NEN) Materials Community of Practice website (https://nen.nasa.gov/web/materials/documents) and possibly other sites.

5.0 Problem, Test, and Test Article Descriptions

5.1 Problem Statement

There are few if any clear, visual, and detailed images of carbon fiber strand failures under tension useful for determining mechanisms, sequences of events, different types of failure modes, etc. available to researchers. This makes discussion of physics of failure difficult.

It was also desired to find out whether the test article-to-test rig interface (grip) played a part in some failures. These failures have nothing to do with stress rupture failure, thus representing a source of waste for the larger 13-00912 investigation into that specific failure type. Being able to identify or mitigate any competing failure modes would improve the value of the 13-00912 test data.

The beginnings of the solution to these problems lay in obtaining images of strand failures useful for understanding physics of failure and the events leading up to failure. Necessary steps include identifying imaging techniques that result in useful data, using those techniques to home in on where in a strand and when in the sequence of events one should obtain imaging data.

5.2 Methods Used; Imaging Techniques Investigated

Carbon fiber strands appear to have considerable variability in failure strength and mode (see examples in Section 6.1). It is at present impossible to predict where a strand will fail. To ensure some number of useful failure images were captured, 26 strands were ultimately pulled to failure in a 5,000 pounds-force (5 Kip) hydraulic tension load frame that had been calibrated for a 1 Kip load range. A displacement rate of 0.05 in/min was used. Excluding load-holds, this gave an approximate 4-minute window over which to perform imaging, with the most-useful information coming from late in that window.

High-speed video (video), digital image correlation (DIC), thermography, and X-ray computed tomography (CT) scanning were used to supply images and begin to reveal failure physics. The high-speed video images were captured using two Phantom® v311 cameras. Each system had a variable focal length lens that was set to a focal length of 300 mm (11.8 inches). The cameras provided configurable resolution of up to 1280 × 800 pixels, which produced 3,200 frames per second (fps), but by reducing the resolution to 1008 × 32, a frame rate of 95,000 fps could be achieved. The DIC system was a VIC-3D Micro™ stereomicroscope system from Correlated Solutions, Inc., which could image 0.2-inch-long sections of the strand at a time with a pixel resolution of 0.002 to 0.006 inches. The microscope was on a traversing stage so that during a test, the loading could be paused and a series of 0.2-inch-long sections could be imaged. Thermography images were captured with a FLIR SC6000, a 3–5 micron (12×10^{-5}- to 20×10^{-5}-inch) infrared camera. The X-ray CT scans were produced by an Xradia 500 Versa three-dimensional (3D) X-ray microscope at the Cornell University Biotechnology Resource Center Imaging Facility.

5.3 Test Article

The finished test article is shown in Figure 5.3-1. Its gage section length (strand section between the grips) was approximately 6 inches.

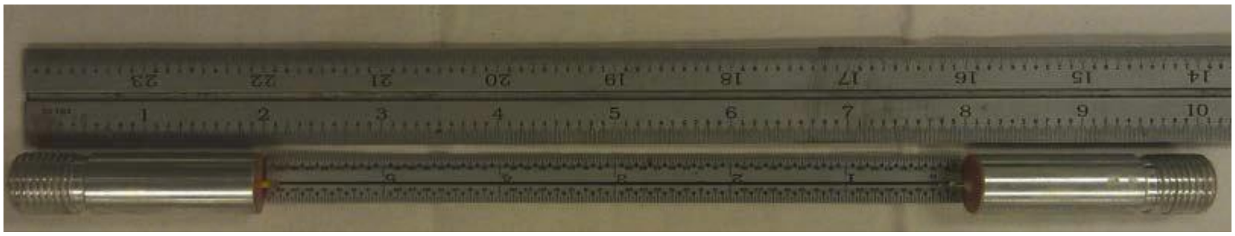

Figure 5.3-1. Composite Strand with Attached Grips

The carbon fiber strand test articles were constructed for NESC assessment TI-13-00912 COPV Stress Rupture Reliability (13-00912). The test articles used were constructed at the MSFC Composite Technical Center (see Figures 5.3-2 and 5.3-3). The test articles were a cylindrical cross-section strand of carbon fibers in a cured epoxy matrix.

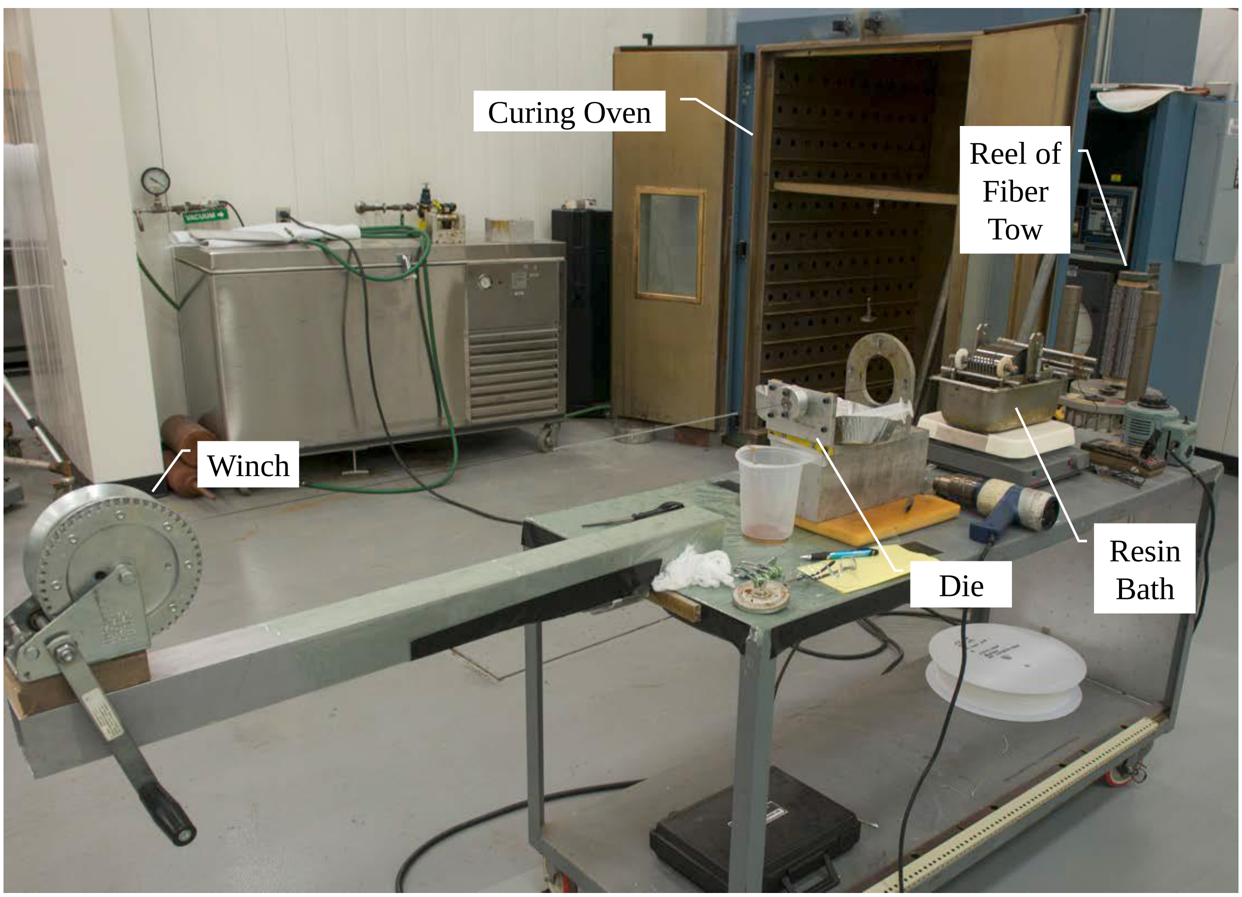

Figure 5.3-2. Strand Manufacturing Setup at MSFC.
The strand is pulled from the reel through the bath through the die using the winch.

Figure 5.3-3. Fabrication of Carbon Strands for Stress Rupture Failure Testing. A winch (right) is used to draw the carbon fiber material through the die (left). Phil Thompson (L) and Chad Hastings (R) demonstrate a preparation step before the test article is cut to length.

A detailed description of fabrication of the test articles will be available in the 13-00912 final report. The general description of strand construction is as follows. Toray T1000 carbon fiber was drawn at 5 lb tension through a heated bath filled with a mixture of EPON™ 828 epoxy resin and EPIKURE™ Curing Agent W. Once the fiber was wetted out, it was sent through a die with a 0.029-inch circular orifice to set the fiber volume. Once pulled through the die, a gel coat of additional resin was added with a syringe for protection of the fiber. The mixture was then pulled through shrink tube to squeeze out any excess resin and to set the final strand diameter. The test article was inserted into heat-shrink tubing. A heat gun was used to shrink this jacket, forcing excess resin from the strand. Finally, the strand was cut to length and cured vertically in an oven with a 0.5-lb weight attached to the bottom of the strand to ensure the strand remained straight during cure.

At the time of this study, the manufacturing process was being optimized and two different shrink tubings were used that squeezed out different amounts of resin. Specimens 8101 through 8206 had a larger average diameter ~0.033 inches while specimens 8402 through 8542 and 5 through 39 had a small average diameter ~0.029 inches. The smaller diameter resulted in a higher fiber volume fraction and was more consistent with the strands used in the 13-00912 assessment.

Test rig interface grips were applied in a lab at LaRC. A schematic of the grip design is shown in Figure 5.3-4.

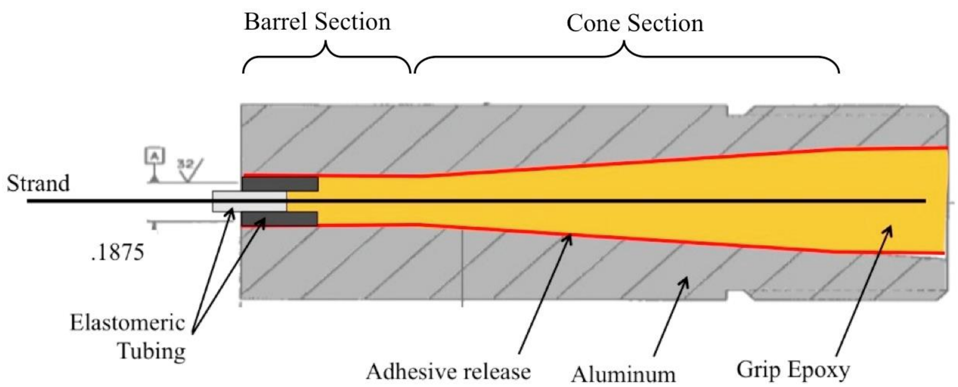

Figure 5.3-4. Schematic of Strand Grip, Cross-section

Construction was an aluminum cylinder with a hole bored through lengthwise to accept the strand. The design diameter of the hole was being optimized at the time these strands were run, so two different bore diameters were used in the barrel section, as noted in the database. Approximately 75% of the central hole's length had a cross-section that increased toward the end, forming a funnel-shaped cone. The end of the grip having the wider hole diameter was threaded to interface with mating connectors on test rigs.

The strand test article was pushed through the central hole of the grip, with the gage section protruding through the hole's narrower barrel end (left, in Figure 5.3-4). A short bushing system made of elastomeric tubing was pushed onto the strand such that it cushioned bending stresses where the gage section protruded through the grip. The bushing system also sealed the end of the grip so that it could be filled with an epoxy and cured in an oven. Prior to being filled with epoxy, the metal grip was sprayed with an adhesive release so that the epoxy would slide against the metal.

Pulling the grips in a tensile test rig causes the cone-shaped epoxy to compress around the carbon fiber strand, more or less evenly and firmly clamping the strand without causing undue high stress concentrations within the gripped section. In practice, it took several refinements to optimize this design so that it gripped the strand adequately. This development work was in its early stages at the time this task was performed, which is believed to be a key reason these tests produced failures at low peak loads (maximum 413 lbf/median 377 lbf) compared to the measured average peak load of 418.9 lbf of the strands used in the 13-00912 assessment. The peak loads in this study may also have been affected by heating from the high-intensity lights needed from some of the techniques and because some of the test had to be paused at a number of intervals in order for readings to be taken.

6.0 Data Obtained

This section describes the data obtained: the measurement systems, resulting information, and spreadsheet data.

Table 6.0-1 shows that a total of 26 specimens were tested as part of this study and indicates which nondestructive evaluation (NDE) technique was used on each specimen. Twenty specimens were imaged with high-speed video, eight specimens with DIC, three with thermography, and a small section of one specimen was imaged with Microfocus CT. In Appendix A, a listing of observations made from each specimen can be found.

Table 6.0-1. Summary of Test Specimens Tested

					Measurement systems used					
Ser. No.	Alt Ser. No.	Failure Mode	Valid Strength	Pre-Damage Evident	Vic (DIC)	High Speed Camera	Camera Frame Rate fps	Micro Focus CT	Thermo-graphy	Notes
8102	B1SP2	Center	Y	N/A	(none)	(none)	(not rec.)	Micro	(none)	1 inch intact section from broken specimen sent to CT only 0.3 in. imaged.
8101	B1SP1	Center	Y	N/A	(none)	HS	32000	(none)	(none)	Some data and references may be incorrectly labeled B2Sp1.
8202	B2SP2	GripF	N	N/A	(none)	HS	64000	(none)	(none)	Failure in grip. Painted white with grey background.
8204	B2SP4	(Not rec.)	Y	Y	(none)	HS	64000	(none)	(none)	Damage early with but continued to take load.
8206	B2SP6	Center	Y	N/A	(none)	HS	64000	(none)	(none)	Failure near but not in grip.
8402	B4S2	Center	Y	N/A	(none)	HS	64000	(none)	(none)	Smaller diameter grip bore.
8404	B4S4	Center	Y	N/A	(none)	HS	64000	(none)	(none)	Smaller diameter grip bore.
8405	B4S5	Split	Y	Y	(none)	HS	64000	(none)	(none)	Smaller diameter. Fiber split bundle split off shortly before failure.
8406	B4S6	Center	Y	Y	Vic	HS	64000	(none)	(none)	Smaller diameter. Failure shortly after hold.
8407	B4S7	Center	Y	Y	(none)	HS	64000	(none)	(none)	Smaller diameter. Damage and fail on reload.
8409	B4S9	Center	Y	Y	(none)	HS	64000	(none)	(none)	smaller diameter damage and fail on reload
8410	B4-SP10	Center	Y	Y	Vic	HS	64000	(none)	(none)	Smaller diameter. Failed at constant load before additional VIC data could be taken no high speed.
8408	B4-SP8	ConeD	N	N/A	Vic	HS	64000	(none)	(none)	Smaller diameter. Cylindar section cracked and debonded from cone.
8513	B5SP13	ConeD	N	N/A	(none)	HS	(not rec.)	(none)	(none)	
8523	B5SP23	GripF	N	N/A	(none)	HS	(not rec.)	(none)	(none)	Significant nonlinear loading before failure failure in grip and then rebound near the opposite grip.
8515	B5(4)S15	Split	N	N/A	(none)	HS	(not rec.)	(none)	(none)	Nonlinear loading curve. Perhaps due to temperature rise lights turned on at 350 lbf.
8542	B5SP42	Center	Y	Y	(none)	HS	(not rec.)	(none)	(none)	Some nonlinear loading evident before failure perhaps due to heat lights turned on at 350lbf.
8525	B5.3SP25	GripF	N	N	Vic	HS	(not rec.)	(none)	(none)	Large diameter grip bore. Vic Failed during hold.
8514	B5.3S14	Split	Y	Y	Vic	HS	(not rec.)	(none)	(none)	Large diameter. Significant strand splitting before failure.
8541	B5.3S41	Center	Y	Y	(none)	HS	(not rec.)	(none)	(none)	Large diameter.
14	B5.5-SP14	Center	N	N	Vic	HS	(not rec.)	(none)	(none)	Fouled inside surface of grip.
31	B5.7-SP31	NoFail	N	Y	Vic	(none)	(not rec.)	(none)	(none)	Specimen did not fail: stopped test to observe splitting damage.
17	B5.6-SP17	Center	N	N	Vic	(none)	(not rec.)	(none)	(none)	Fouled inside surface of grip. Some failure inside grip as well. Vic performed without load holds.
39	B5-6S39	GripD	N	Y	(none)	(none)	(not rec.)	(none)	Thermograpy	Fouled inside surface of grip.
5	B5-6SP5	Center	N	N	(none)	(none)	(not rec.)	(none)	Thermograpy	Fouled inside surface of grip.
27	B5-6SP27	GripD	N	Y	(none)	(none)	(not rec.)	(none)	Thermograpy	Fouled inside surface of grip.

6.1 Database

The information package containing the videos, presentations, papers, etc. mentioned in this paper will be made available on the NEN Materials Community of Practice website (https://nen.nasa.gov/web/materials/documents) and possibly other sites.

A total of 26 strands were tested. A database, Imaging Study Database.xlsx, summarizes key strand information and includes additional information not included in Table 6.0-1.

Measured strength data are not representative of the strand population ultimately tested in 13-00912 nor of T1000 strands for at least two reasons:

1. These specimens were tested while the manufacturing and gripping techniques were in early development. Significant improvements were made over the course of test article development.
2. At least some of the imaging systems evaluated probably had an effect on strand strengths. In particular, bright lights used for high-speed video and VIC heated the strand, likely affecting the strand's epoxy matrix and quite possibly other parts of the test article. The testing of some of the strands also was paused periodically in order to take readings with the DIC system. These holds at high stress level are also believed to have affected the measured strength of the strands.

Although the measured failure load values are not representative of the larger strand study and should not be used for design or other critical purposes, the values are given for completeness. The failure modes themselves appear to represent failure types seen in 13-00912, though the frequencies of occurrence of the undesirable modes competing with the stress rupture mode are diminished in that larger study. This is due to improved strand manufacturing and gripping processes.

The column marked "Valid Strength" in Table 6.0-1 indicates whether the failure was due to a mode that appeared to be a strength failure representative of the strand's strength. Valid strength failure values can be used as reported in calculations. "Invalid" failures were associated with a flaw in grip design, alignment, strand manufacture or other cause. These invalid failures should be treated as runouts, or censored points, when calculating mean strengths because they broke below their true ultimate tensile strengths. This mathematical correction is necessary for best-practice engineering strength characterization of the strand population.

The archived database contains more information that is presented in Table 6.0-1 such as gripping information and failure strength.

Gripping information was collected and is included in the database, though it likely has little impact on failure mode and is only supplied for completeness. The grip epoxy cure oven batch is noted. Large versus small bore refers to the size of the hole through the grip. All were gripped by the same technician.

The date of each strength test is recorded. The peak load is also listed. Some are higher than the value in the *Strength* column by the value from the *Zero Load* column. That latter column refers to the post-test residual load value shown on the pull tester's readout; it was assumed that this is a bias that should be subtracted from the peak load when the strand broke.

Observed failure modes are as follows.

Center: failure (breakage) occurs clearly within the gage section, between the grips. There are no anomalous slippages or other obvious issues that could imply a failure mode not reflective of a nominal failure event. Strand center material is missing after test. A failure occurring primarily in the center of the strand is normally considered a valid failure. Examples of post-test specimens exhibiting center failures are shown in Figure 6.1-1. An example of the video-imaged failure sequence (SN# 8101) is shown in in Figure 6.1-2. Although some initial damage occurs just before failure, the main tension break occurs remote from the initial damage. The main tension break is followed almost immediately by a compressive recoil break near a grip, producing a clean cut across the strand near one of the grips. With the fiber severed in two spots the rest of the strand collapses sending fibrous material toward both grips, which often embeds into the elastomeric material as shown in Figure 6.1-1.

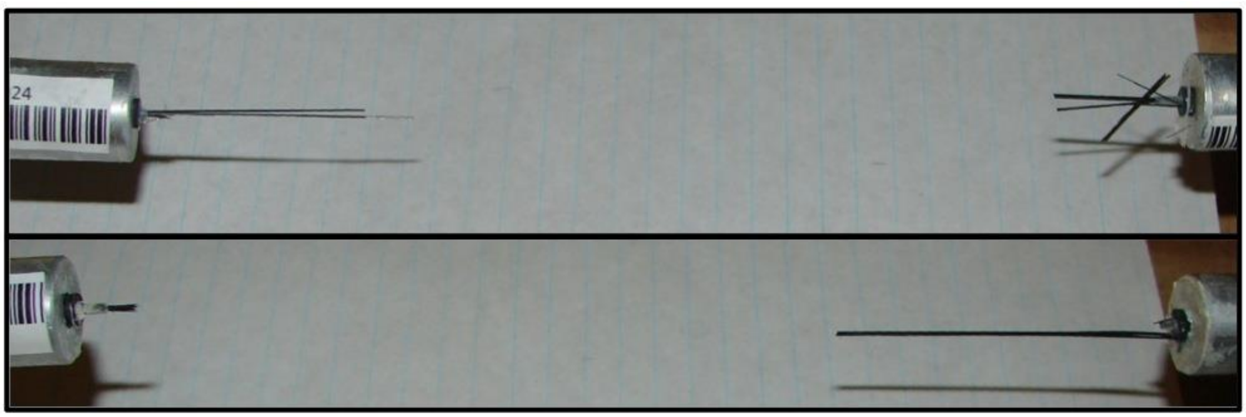

Figure 6.1-1. Images of Broken Strands after "Center" Failure (example strands, not part of this study)

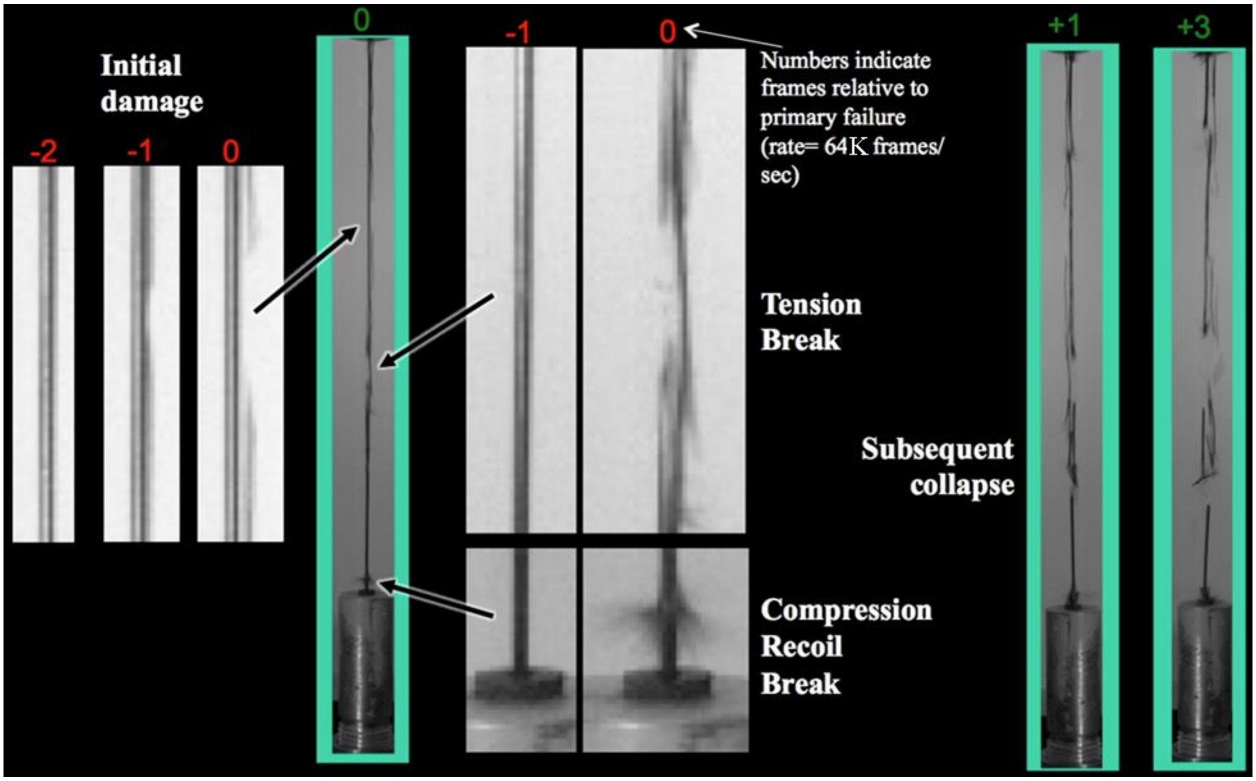

Figure 6.1-2. High-speed Camera Images Showing Sequence of Failures in "Center" Failure Mode (S/N 8101)

GripF: grip failure; failure of the strand in the grip region (see Figure 6.1-3). These failures could indicate either damage due to gripping or the weakest point of the strand did randomly occur in the grip. Because of the uncertainty in this failure mode, GripF failures are usually considered invalid even if the failure load value is relatively high.

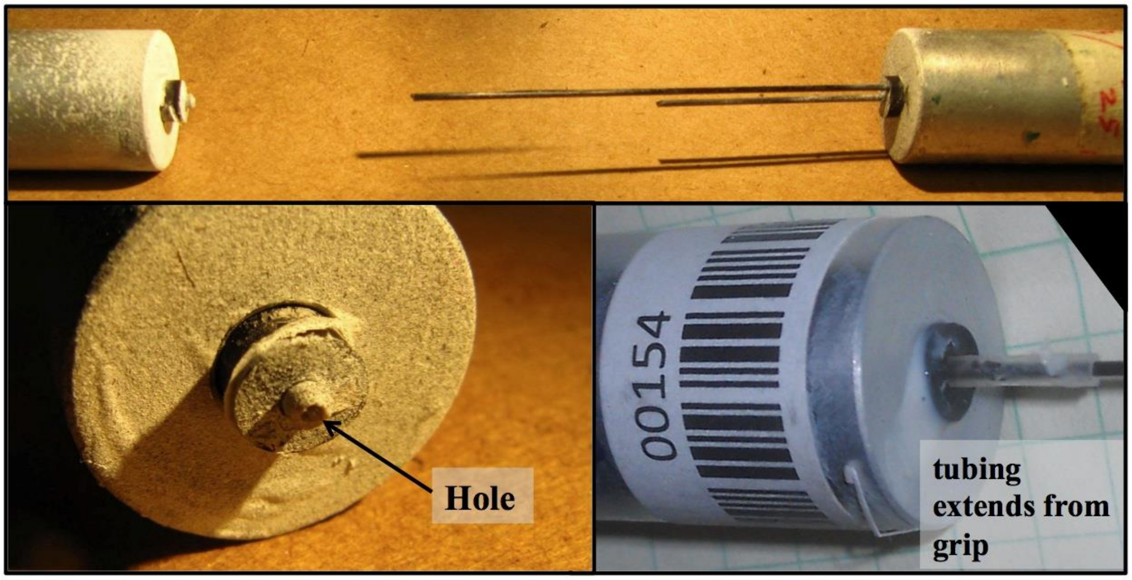

Figure 6.1-3. Images of Broken Strands After "GripF" Failure Mode

Split: strand splits in the gage region rather than making a sharp, clean break. The specimen tends to remain somewhat intact with long longitudinal splits down its length. A Split is normally considered a valid failure. Images of post-test specimens from "Split" failure mode are shown in Figures 6.1-4 and 6.1-5. Notice that even though the failed specimen looks distinct from a "center" failure, the initiation may be similar with a different progression mechanism, such as a primary tension break occurring within the gage section.

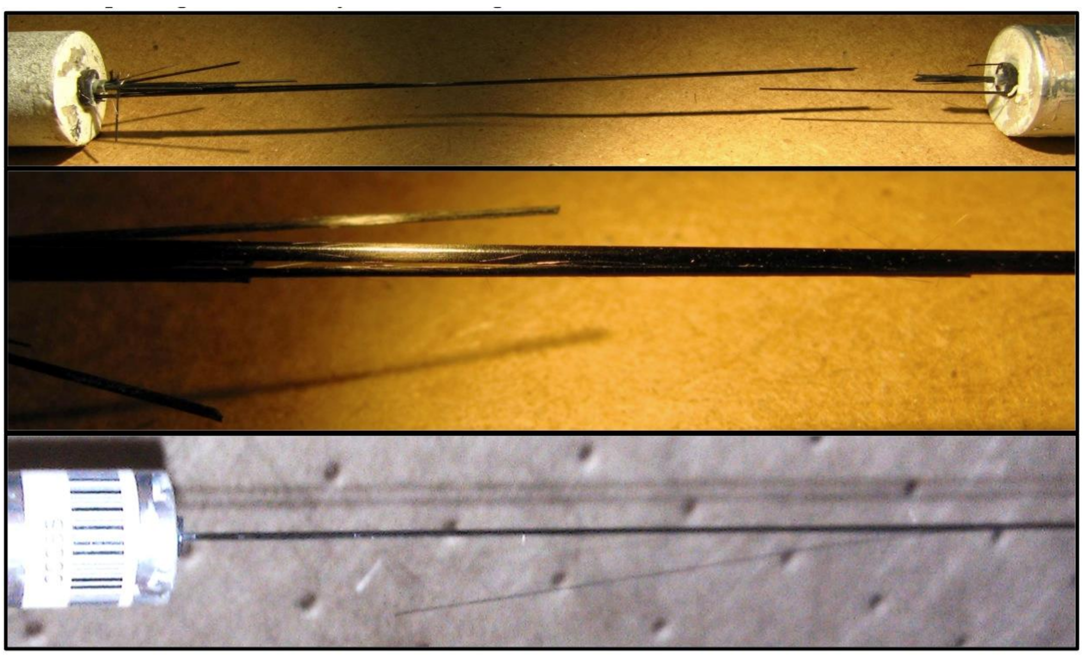

Figure 6.1-4. Images of Broken Strands after "Split" Failure Mode

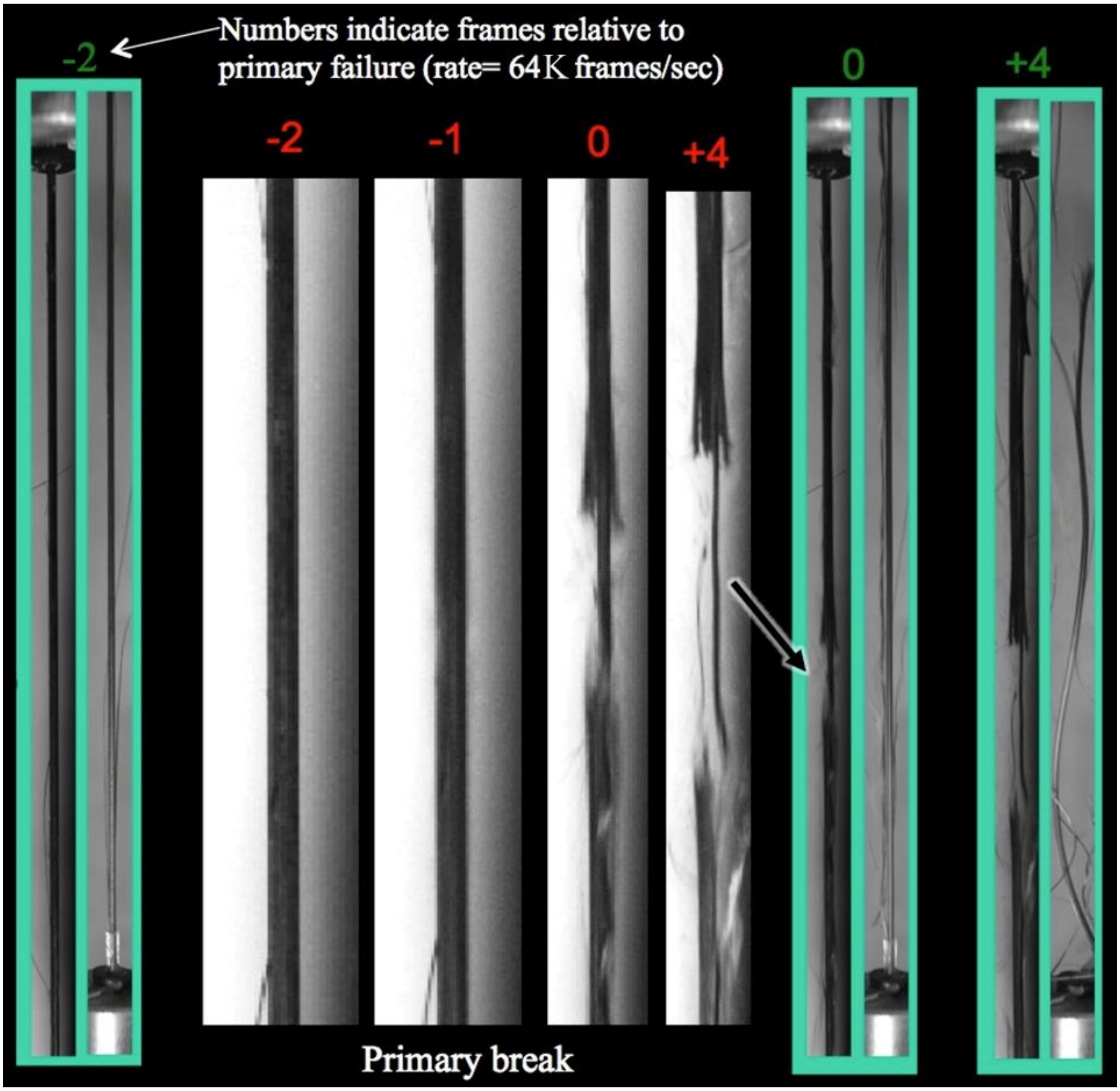

Figure 6.1-5. Failure Sequence from SN 8405 Characterized as "Split"

ConeD: cone debond; the strand debonds from the epoxy plug in the grip allowing the strand to pull out from the grip (see Figure 6.1-6). Evidence might include cracking between the cone and narrow (barrel) section of the plug. Normally considered an invalid failure, ConeD generally results in failure at a lower-than-expected load value than strands broken in the gage region.

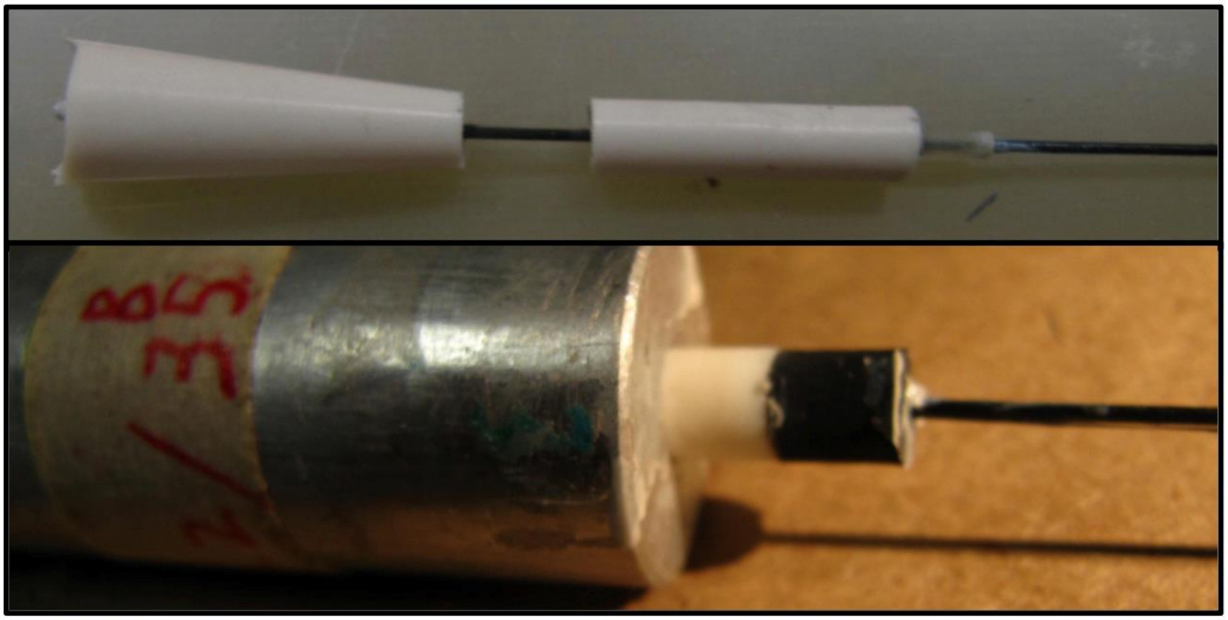

Figure 6.1-6. Images of Specimen Associated with a "ConeD" Failure Mode

GripD: grip debond; strand debonds from grip epoxy and slips in the grip. This is considered an invalid mode. The strand may not fail, but often the energetic release causes a subsequent compression recoil failure of the strand similar to that seen in Figure 6.1-7.

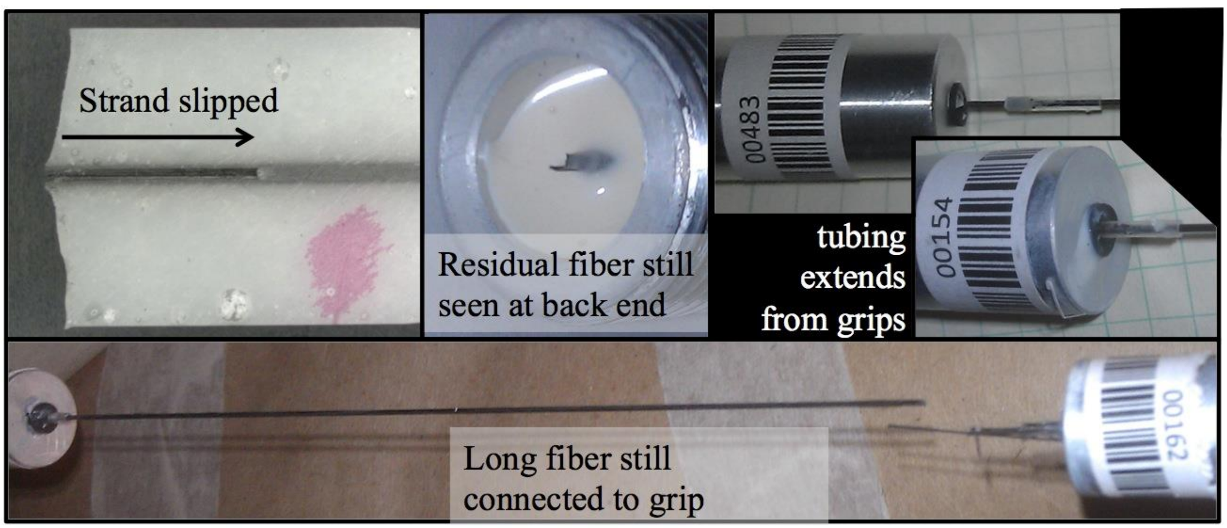

Figure 6.1-7. Images of Broken Strands after "GripD" Failure Mode

NoFail: strand was not loaded to failure.

Generally, if a strand broke cleanly in an acceptable failure mode, it was judged to be a valid strength failure. That is, had these data come from a more mature manufacturing and gripping process, its load data would have been used in strength characterization analysis. The notes describe several strands that experienced a "fouled" grip application. The inside surface of these grips were found to have been significantly marred during fabrication. Without a clean surface that would allow the epoxy to slide in the grip, the grip could not function as intended. Therefore, these strength values were suspect even if the failure mode otherwise appeared valid.

Pre-damage refers to some damage event occurring before failure: for example, some individual fibers breaking before final catastrophic failure of the strand.

6.2 Measurement Systems

The information package containing the videos, presentations, papers, etc. mentioned in this paper will be made available on the NEN Materials Community of Practice website (https://nen.nasa.gov/web/materials/documents) and possibly other sites.

6.2.1 High-speed Video Imaging

A Phantom® v311 video system was used to capture data as strands were loaded to failure. The recorded .avi files are included in the folder "High Speed Test Records" in the information package.

6.2.2 Digital Image Correlation (DIC)

Figure 6.2-1 is a photograph of the DIC setup showing the stereo microscope used to measure strains in a composite strand. Cameras for high-speed imaging are also shown.

The DIC measurement system was used to look at deformation of the strand under tension compared to its at-rest state, thus providing the tensile strain under load. Most measurements were performed during load "holds." It was observed that during these holds, a period of slow load relaxation occurred in the test article during the measurements process.

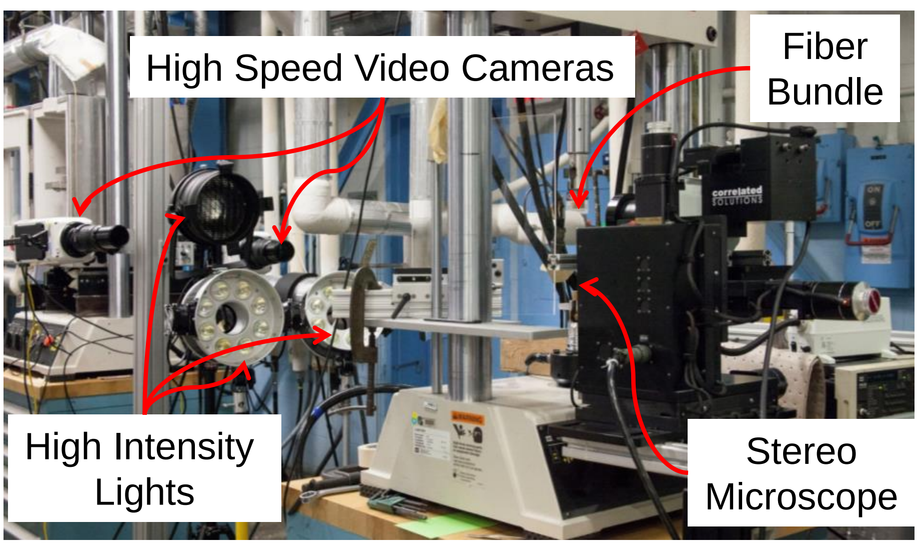

Figure 6.2-1. Photograph of the DIC Setup

It was desired to find out whether precursors to failure could be found in the strain data. It was hypothesized that these locations might be evident as emerging strain localization. A localized area of strain increase was observed but did not closely correspond to the apparent failure location in at least two strands, S/N 8410 (B4-SP10) and S/N 14 (B5.5-SP14). It was concluded that while the method is useful for measuring strain in a carbon fiber strand under tension, it may not be useful for predicting failure or the region where failure initiates without further development.

Most DIC measurements were performed during "holds"; that is, the load frame was paused to take measurements. This actually resulted in a period of slow and slight unloading in the test article during which the measurements were performed.

A number of lessons learned were identified intended to assist future researchers and technicians. A full accounting of the VIC-3D Micro™ measurement system as applied in this investigation is in the paper "Carbon Fiber Test Report Summary" [ref. 1] attached to the complete information package this report summarizes. Datasets from DIC analysis are also in the package contained in the folder "High Speed Test Records."

6.2.3 Thermography

A FLIR SC6000 thermographic imaging system was used to obtain these data. Video records of thermography tests are included in the package. Figure 6.2-2 shows the measurement system setup.

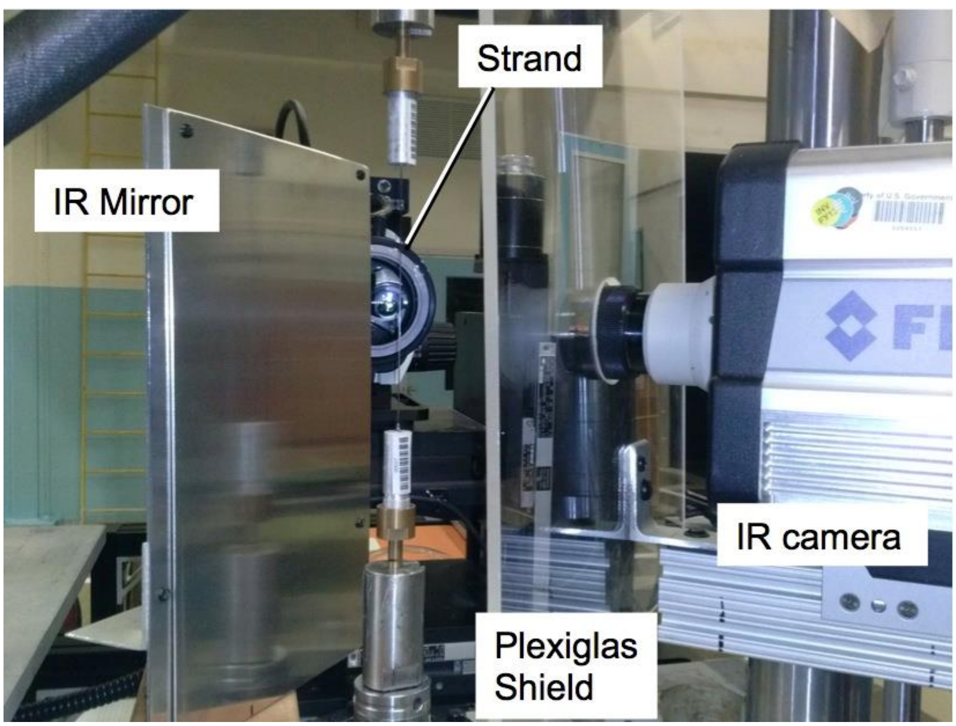

Figure 6.2-2. Experimental Setup for Thermography Data Collection

It was found that thermal transients, many quite pronounced, were observed during strand loading, at least some of which appeared to be associated with bundles of fibers failing in tension. It was concluded for this reason that this measurement system may be of value for research into events involved in failure progression. Figure 6.2-3 depicts example thermography showing several high-energy events occurring as much as 11 seconds before final failure of the specimen.

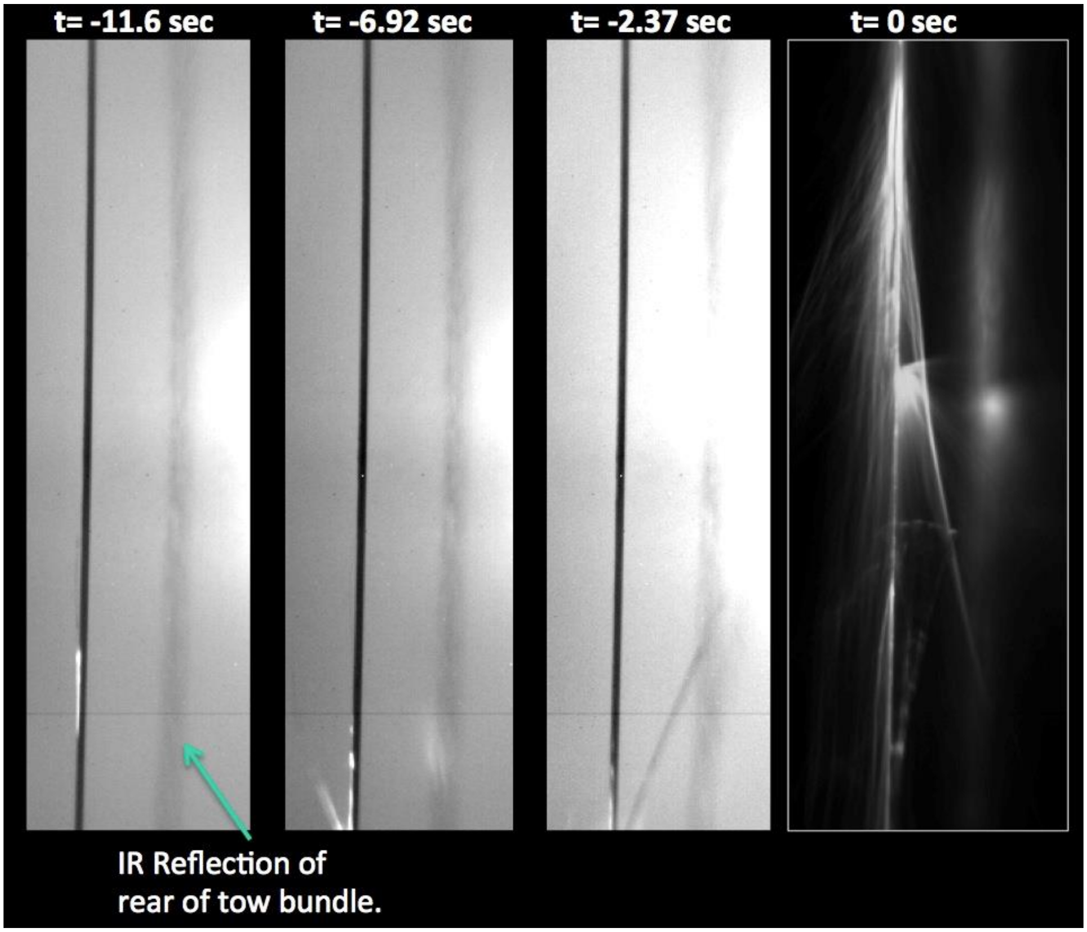

Figure 6.2-3. Example Thermography Images From Specimen S/N 5

A presentation Fiber Tow Thermography Testing (9_19_2013 tow thermography results v2.pptx) [ref. 2] in the information package summarizes the work. Videos originally used in the presentation are also included in the information package.

6.2.4 Microfocus Computed Tomography (CT)

Strand S/N 8102 was imaged after tensile failure test using Microfocus CT.

It was found that Microfocus CT was able to characterize a small region of material in great detail as shown in Figure 6.2-4, but only small regions could be scanned at a time at a resolution high enough to see damage in individual fibers. Individual fibers' locations can easily be traced down a strand and breaks in individual fibers can be detected. Details such as the relative proximity of these breaks to each other and extent and path of longitudinal cracks can be understood. Fiber spacing and resin-rich areas can be characterized and even quantified. It would seem that although the expense and time associated with this type of imaging can be high and therefore only a small section of one strand was imaged, the understanding gleaned from the scans may prove valuable once a characteristic damage state is identified. These data could be useful for informing increasingly high-fidelity physical simulation models such as finite element models detailed to the fiber level.

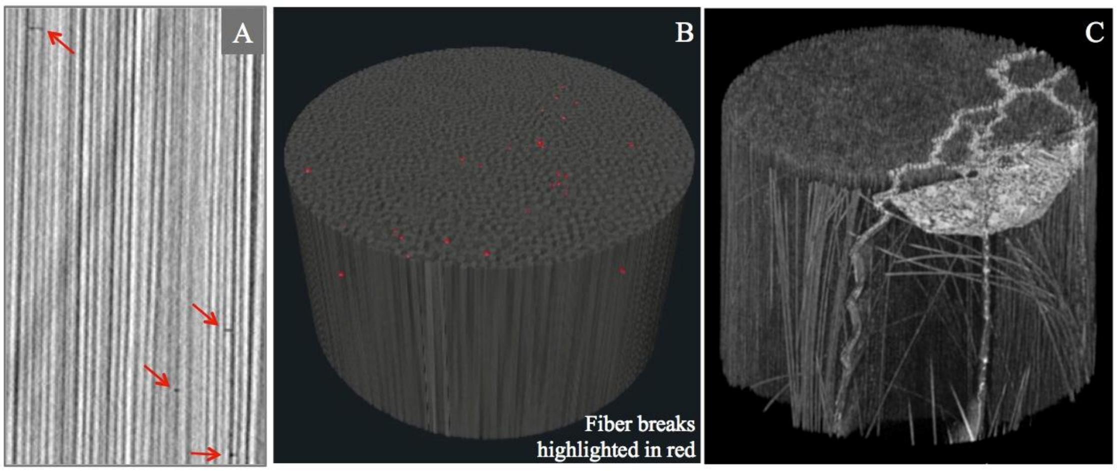

Figure 6.2-4. Images from Microfocus CT Scans Showing A) Fiber Breaks in a 2D Slice of Strand Material, B) Fiber Breaks Scattered within a 3D Volume of Strand, and C) Axial Splits with a Strand

A detailed report of methods and findings [ref. 3] along with a brief set of slides, 3D X-ray Microscopy of Single-Strand Tensile Test Specimen: Exploratory Data [ref. 4] are available in the information package. Three video files created from the scans, each highlighting different aspects of strand damage, are also included:

- Video_1.mov and Video_2.mov explore fracture surfaces. These augment still images in the presentation.
- fiber_breaks.mpg highlights and locates in 3D space individual fiber breaks within a seemingly intact section of strand.

6.2.5 Other Data

Also included in the information package:

- Still post-test images and other views such as the images shown in Figure 6.2-5. This figure shows the post-failure ends of specimen SN 8407 and the longitudinal splitting that can occur in a specimen during the failure process. The origin of this spitting can be understood by referring to high-speed imaging as shown in Figure 6.2-6.

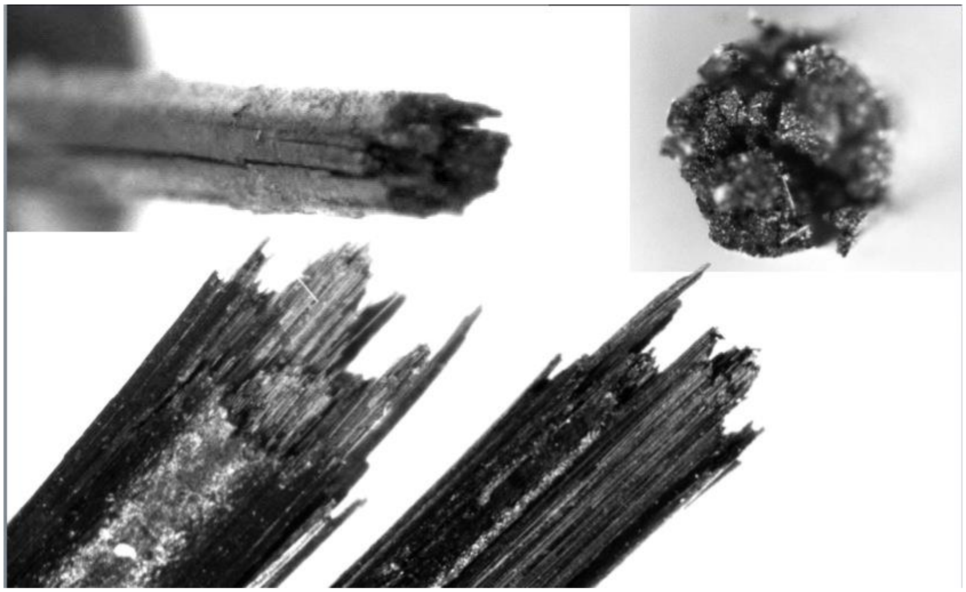

Figure 6.2-5. Fractured Ends of SN 8407 Showing Multiple Axial Splits

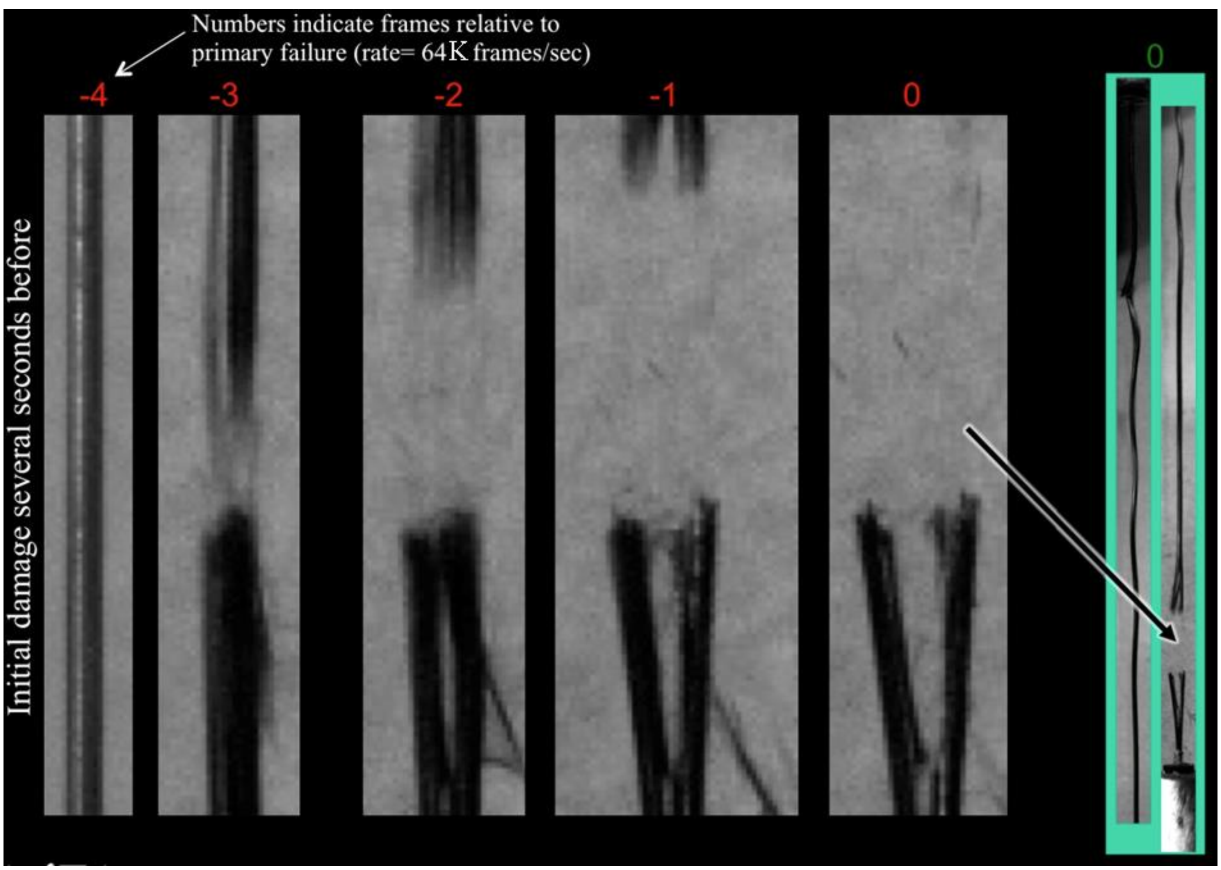

Figure 6.2-6. High-speed Imaging of SN 8407 Showing Dynamic Tension Failure Splitting the Failing Strand Open

- Load displacement data. An example load displacement chart is shown in Figure 6.2-7. As seen in the example, there are generally two discrete events per trace showing a rapid load decrease. These correspond to "grip slips," events in which the epoxy plugs attached to the strand become debonded from the grip walls (not the strand) under load, slip slightly toward the gage section, and reseat abruptly. This signals a constriction of the plug, providing constraint to keep the strand itself well bonded to the epoxy cone. These excursions are an indication that the gripping system is behaving as it should, and normally not an indication of any damage occurring in the strand itself. Some displacement charts from other specimens do show some discrete load drops closer to the final load that may indicate damage to the strand.

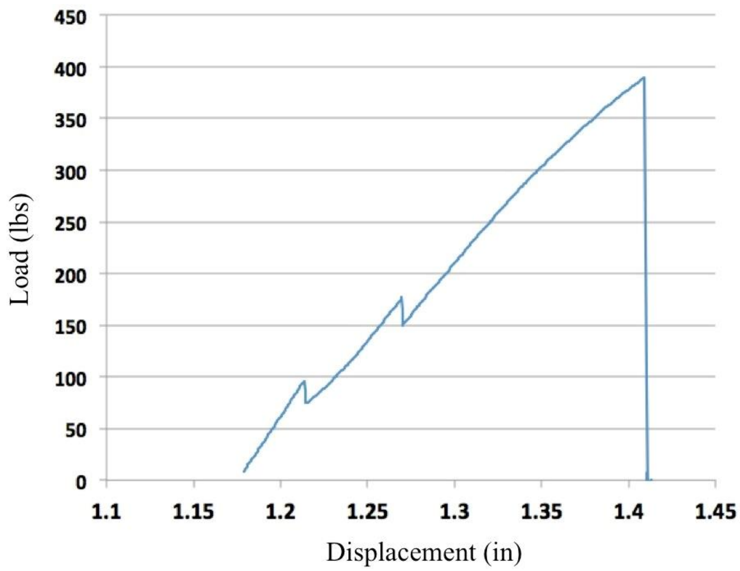

Figure 6.2-7. Example Load Displacement Chart from Specimen SN 8206 Showing Grip Slip Events

7.0 Discussion

The objective of this study was to improve the understanding of the physics of strand failures by applying several imaging systems. Four different NDE techniques were employed to this end.

The most significant success was in documenting the sequence of failures during a GripD-type failure. In a GripD failure, the strand becomes debonded from the gripping epoxy and slides out of the grip. The failure is often dynamic enough that a shock wave travels down the strand creating a compressive failure near the opposite grip. These tests are invalid strength tests because the failure is precipitated by the failure between the strand and the grip epoxy, which does not directly relate to the strength of a strand. Because the specimen may have broken in the gage region, simple inspection of a failed specimen may miss the precipitating event in the grip. Seeing that the strand has pulled partially from the grip often requires a detailed inspection. It was only through the inspection with high-speed video that the compression recoil failure was understood as seen in Figure 6.1-2. By understanding that the GripD failure mode produces an invalid strength value, the data point can either be removed from the data set or, more properly and accurately, censored in analysis, indicating that the true strength is somewhat higher than the measured strength. Accounting correctly for this failure by a competing failure mode will affect the determined average strength, making it more accurately reflect the strands' true average strength.

The goal of the 13-00912 assessment that will be using test articles comprised of the type of strand and grip used in this investigation is to study stress rupture, a composite failure mode where failures can occur after a period of time being held at a constant load. Stress rupture is of critical concern for COPVs where a structural failure would likely be catastrophic to a mission.

To study stress rupture, strands will be tested for a period of time at an elevated sustained load compared to use conditions and the number of failures counted. Strands will be tested at a number of stress levels so that an adequate number of failures are obtained. The results will be used to extrapolate to predictions of failures at stress levels where structures are normally operated. Extrapolations based on these accelerated load conditions are necessary because testing at use conditions cannot be reasonably performed: failure rates for vessels are often expected to be less than one in a million in missions lasting 10 years or more.

Even at accelerated load conditions, testing requires a large number of strands and is thus expensive. If failures due to gripping or other competing failure causes get mixed with valid failures, the reliability predictions could be significantly affected, representing a waste of test time and resources. Improperly including failures in analysis due to invalid modes will tend to decrease the estimated reliability, which would produce conservative results. However, the stress level used in calculation is typically normalized by average strength, calculation of which is also affected by competing failure modes. Depending on the relative effect of grip failures on strength versus stress rupture, the fictitious results could be conservative or un-conservative. Because the failure modes were better understood through the work performed in this investigation, this problem can be mitigated.

One original hope for this study was that by studying strength failures, clues to the underlying cause of stress rupture could be determined. Unfortunately, this effort was not as successful. The key to attaining this goal was to see damage develop as loading was occurring and then stop the testing so that the damage state could be carefully studied. If the underlying failure mechanics can be understood, then perhaps it could be mitigated, significantly improving reliability.

One of the larger challenges with stress rupture testing (as with strength testing) is that the failure events tend to be catastrophic, leaving little after the fact to examine to determine failure cause, location, or other information. Using high-resolution DIC, localized strain during the loading cycle was successfully tracked. However, such a localization was found in only a couple of the tested specimens (S/N 14 & 8410) in this study. In the sole case in which failure was captured on high-speed camera after a high-strain region developed (S/N 14), the failure did not coincide with the location of high strain. The DIC measurements required the test be repeatedly paused so that the series of images along the length could be captured. Tests that normally lasted a few minutes took several hours to complete when localized strains were recorded. Also, because of the extra personnel involved in setup, operation, and data processing, this technique proved to be an expensive method and could not be employed on many tests. The pauses in loading combined with the heating from the intense lighting required for both DIC and high-speed imagery likely also affected the progressions to failure. Finally, although DIC was able to track localized strain, a characteristic strain hot spot leading directly to failure was not identified. This could indicate that the critical region was localized elsewhere, occurred beneath the surface, or developed too quickly to be discerned with DIC. Overall, this technique requires considerable work before it can be shown to be useful in this application.

The program was planned with just high-speed imaging and DIC, and the bulk of the testing was done with these techniques. However, thermography and Microfocus CT both show significant promise. Thermography was interesting because it could be employed without high-intensity lighting and without load pauses. Although the results are not as precise as the high-resolution DIC, a high-energy event prior to ultimate failure could be captured. The high-intensity indications are presumed to be fiber breaks. But again, it was not clear that a high-energy event on the strand surface led to the failure of the specimen. So, for instance, we were not able to use this technique to halt the test to remove a specimen to more-closely examine a critical damage state just before failure.

Microfocus CT scans were produced from failed specimens after removal from the load frame. Microfocus CT may be available with loading stages, but the time required to produce a scan – though decreasing with improving technology – was significant, making it currently impractical as a real-time imaging method. Nevertheless, Microfocus CT demonstrated the ability to image minute damage in 3D. So if a characteristic damage state could be identified that is leading to failure, the Microfocus CT imaging would be invaluable in understand the nature of that failure mode. With the current results for a single strand, distributed fiber breaks and other hints regarding failure progression and effects were clearly evident. Additional study using this imaging technique, may reveal how these fiber breaks develop and interact.

Although a characteristic failure mode leading to failure was not identified in the study, tracking the various failure modes during the larger stress rupture study may provide clues to the underlying mechanism that results in early failures. In the strength results gained during the 13-00912 assessment using the gripped strands optimized using, in part, information from this study, the majority of the failures have been characterized as center failures. If it is found that the proportion of competing invalid failure modes changes during stress-rupture testing, it would be a clue to what causes some early failures that reduce system reliability. By identifying the different failure modes in this study, correctly identifying competing failure modes in the larger stress-rupture study was made possible. This will allow correct accounting for failures in invalid modes during analysis, leading to more accurate estimates of reliability.

8.0 Findings, Observations, and NESC Recommendations

8.1 Findings

The following findings were identified:

F-1. High-speed video revealed several different possible strand failure mechanisms.

F-2. Certain test article failure modes exhibit failure event sequences and other characteristics different from valid strength failures, making the resulting strength or stress rupture data invalid without proper accounting of the various failure modes during analysis.

F-3. Failures that initiated in the grips that would be considered invalid can result in subsequent failures within the gauge section and could therefore easily be mistaken for valid failures.

F-4. The DIC and high-speed imagery systems used required high light levels, which caused thermally induced changes in a test article.

F-5. DIC at high magnification required pausing the test to gather data, which complicated use of the method for understanding strand failure characteristics.

F-6. CT was found to have sufficient resolution to identify, track, and model relative locations of individual fibers over relatively small strand segments.

F-7. Thermography revealed fiber breakage events not necessarily noticeable as such in the load trace and did not require high light levels or pauses to the test.

F-8. DIC appears to show promise for identifying strain changes as a strand is loaded.

F-9. Thermography, DIC, and possibly CT showed that damage may be occurring in several places along a strand's length as it is loaded, but these locations may not be the eventual failure location.

8.2 Observations

O-1. Further development of CT analysis algorithms could allow future failure analysis and modeling at the fiber level within a strand of fibers.

8.3 NESC Recommendations

No recommendations were identified.

9.0 Alternate Viewpoint

There were no alternate viewpoints identified during the course of this assessment by the NESC team or the NRB quorum.

10.0 Other Deliverables

An information package containing this report along with all the imagery and accompanying presentations and papers will be made available on the NASA Engineering Network (NEN) Materials Community of Practice website (https://nen.nasa.gov/web/materials/documents). The intention is to make it more broadly available if a suitable public repository is identified.

11.0 Lessons Learned

No applicable lessons learned were identified for entry into the NASA Lessons Learned Information System (LLIS) as a result of this assessment.

12.0 Recommendations for NASA Standards and Specifications

No recommendations for NASA standards and specifications were identified as a result of this assessment.

13.0 Definition of Terms

Finding	A relevant factual conclusion and/or issue that is within the assessment scope and that the team has rigorously based on data from their independent analyses, tests, inspections, and/or reviews of technical documentation.
Lessons Learned	Knowledge, understanding, or conclusive insight gained by experience that may benefit other current or future NASA programs and projects. The experience may be positive, as in a successful test or mission, or negative, as in a mishap or failure.
Observation	A noteworthy fact, issue, and/or risk, which may not be directly within the assessment scope, but could generate a separate issue or concern if not addressed. Alternatively, an observation can be a positive acknowledgement of a Center/Program/Project/Organization's operational structure, tools, and/or support provided.
Problem	The subject of the independent technical assessment.
Recommendation	A proposed measurable stakeholder action directly supported by specific Finding(s) and/or Observation(s) that will correct or mitigate an identified issue or risk.

14.0 Acronyms List

3D	Three Dimensional
COPV	Composite Overwrapped Pressure Vessel
CPVWG	Composite Pressure Vessel Working Group
CT	Computed Tomography

DIC	Digital Image Correlation
FOV	Field of View
fps	Frames Per Second
HS	High Speed
Kip	1,000 Pounds-Force
LaRC	Langley Research Center
MSFC	Marshall Space Flight Center
NDE	Nondestructive Evaluation
NESC	NASA Engineering and Safety Center
S/N	Serial Number

15.0 References

1. Dawicke, D. S. (2013). *Carbon Fiber Test Report Summary: High Speed and Digital Image Correlation Measurements.* Hampton, VA: Analytical Services and Materials, Inc.
2. Burke, E. (2013). *Fiber Tow Thermography Testing.* NASA Langley Research Center, Nondestructive Evaluation Sciences Branch, Hampton, VA.
3. Czabaj, M. W., Riccio, M. L., & Whitacre, W. W. (2014). *Three-Dimensional Imaging and Numerical Reconstruction of Graphite/ Epoxy Composite Microstructure Based on Ultra-High Resolution X-Ray Computed Tomography.* NASA Langley Research Center, Hampton, VA. Retrieved from http://ntrs.nasa.gov/archive/nasa/casi.ntrs.nasa.gov/20150000580.pdf
4. Czabaj, M. W. (2013). *3D X-ray Microscopy of Single-Strand Tensile Test Specimen: Exploratory Data.* PowerPoint presentation, NASA Langley Research Center, Hampton, VA.

16.0 Appendices

Appendix A Brief Observations on Individual Strands' Imagery

The information package containing the videos, presentations, papers, etc. mentioned in this paper will be made available on the NEN Materials Community of Practice website (https://nen.nasa.gov/web/materials/documents) and possibly other sites.

This section will discuss observations found notable through evaluation of each strand's data. HS = high-speed video; VIC = VIC digital image correlation; CT = Microfocus computed tomography. Each frame in the original imaging resulted in a frame in the video file, so where imaging frame rates are available, event timing can be approximated. Strands are approximately 6 inches between grips (gage section).

The observations listed in this section are meant to be used only as a catalog so that experts can quickly identify for further study imagery relevant to their own needs.

S/N 8101/B1SP1. HS, failure in strand center (gage section, between the grips). 32k fps camera speed in video image B1-SP1_Short.avi was found too slow to clearly catch initial failure.

- Frame 19: Failure initiated between frames 18 and 19, probably ~4 inches from the left grip as a separation of a group of fibers.
- Frame 20: Most or all of the rest of the strand breaking approximately 2.5 inches from the left grip. Fracture ends of both fractures pull away from each other; a large compression collision event is evident close to the left grip and the originally failed fiber bundle is buckling and showing a number of compression collisions.
- Frame 21: Several other strand breaks seen. Both end segments of strand retreating into respective grips, termed "Robin-Hooding," also seen in still images such as IMG_5338.JPG.
- Frame 26: Strand seen shattered into large-ish, ~1-inch segments and many smaller pieces, most also split longitudinally into slivers. Trajectories slightly chaotic, but focused toward grips rather than outward. Segments colliding with grips shatter into very small pieces.

S/N 8202/B2SP2. HS 64k fps, appeared to fail inside the grip (GripF). Increased camera speed reveals increased detail in B2-SP2_Short.avi. Painted white to attempt to increase contrast and detail.

- Frame 2: Failure evident at left grip.
- Frame 3: Separation on left end; compression failure near right grip. Clear evidence of at least one subgroup of fibers pulling free from main strand bundle at left end.
- Frame 4: indications of paint releasing along entire strand. Small fiber subgroup noted in Frame 3 appears to have lower velocity/ energy than rest of strand.
- Frame 11: Strand separating into individual fibers. Light-colored paint releasing with significant radial displacement compared to strand fibers. Leftmost end of main fiber bundle beginning to fray outward.
- Frame 14: Beginning of buckling wave traveling down-strand from right grip.
- Frame 25 (approximate, off-screen): main fiber bundle fractures in bend closest to right grip after complex, violent buckling near right grip.
- IMG_5359.JPG shows aftermath of failure. Note almost no strand material remains attached to the grips.

S/N 8204/B2SP4. HS 64k fps. Damage to strand occurred early in tensile test; strand continued to accept increasing load, but ultimately failed at a relatively low load. Video file B2-SP4_short.avi:

- Frame 5: Failure evident, but appears to occur out-of-frame at right, possibly within the grip (failure mode not recorded for this reason).
- Frame 6: Failure clear.
- Frame 7: Strand appears to shatter into individual fibers or small bundles from right grip to approximately 3 inches from right grip. Several compression failure sites may be seen. Shattering lessens from that point toward left grip, with strand from left grip to

~1.5 inches little affected and one or more possible small, sharp buckles occurring at the interface.
- Frame 8: Strand breaks at first buckled region near left grip. More small compression sites evident in rightward segment. Clear radial velocity seen in strand fragments centered 1.5 inches from the right grip.
- Load time history B2-SP4.xlsx shows clear unloading event at 323.8 lbf, a decrease to 278 lbf, then final failure at 321.85 lbf.
- Post-test still IMG_5351.JPG shows the nearly intact strand portion remaining at the left grip, while IMG_5354.JPG shows longitudinally split fragmented remains Robin-Hooded into the black elastomeric strain relief portion of the right grip.

S/N 8206/B2SP6. HS 64k fps. Center failure near, but not inside, grip. Video B2-SP6_short.avi may reveal spirally arranged fiber tows down strand, though this does not seem likely due to manufacturing method.

- Frame 3: Slight leftward acceleration of strand.
- Frame 4: Failure site evident near right grip as a short region of increasing diameter.
- Frame 5: Compression events mid-strand and at left grip.
- Frame 6: Small group of fibers separating from large strand segment nearer right grip.
- Frame 7: Two large main strand segments rather than small bundles are formed and remain mostly intact for duration of filmed portion of event.

S/N 8402/B4S2. HS 64k fps. Painted white. Center failure in a smaller-diameter strand. Two cameras used, each capturing notionally half of the strand. Evident damage occurred before failure, termed “pre-damage.”

- B4-SP2_11855_short.avi: view of one grip end.
  - Frame 8: Failure evident. Failure site appears to be highlighted by paint fragments being ejected in a particular starburst-like pattern nearly mid-frame. However, the strand itself is difficult to see.
  - Frame 10: Failure site appears to be a sharp, discrete cross-strand fracture at or near center of the paint starburst. Little rightward displacement of the strand evident from this time on. Leftward strand segment moves leftward until it is absent from frame.
  - Frame 11: Rightward strand section visible, showing fairly fine fraying from the fractured end at least 1 inch toward the grip. Fraying does not involve entire section to grip.
- B4-SP2_11853_Short.avi: view of opposite grip end. Focus is significantly less sharp than other view.
  - Frame 8: Failure evident, but location is in the other camera’s field of view (FOV).
  - Frame 11: Compression buckling evident at grip.
  - Frame 20: Buckling involves entire FOV.

- The "long" video files capture more information on fragment shapes, trajectories, and event sequence timing.
- There are a number of still close-ups of a strand end post-test showing the fracture surface and longitudinal splits. These are named Batch4 Spec2*xxx*.jpg.

S/N 8404/B4S4. HS 64k fps. Painted white. Center failure at relatively, but not remarkably, low value. Strand appears to fracture piecewise over a significant period of time rather than in a large, fast catastrophic event or sequence of events. Video shows significant portion of strand split from balance of strand and fractured near one grip, but remaining diminished strand still carried load.

- B4-SP4_11853_Short.avi. Split, fractured fiber bundle clearly visible. Freed bundle displaced below the strand retaining the white surface paint. Intact fibers without the white surface paint just visible in the shadows. Fracture has a stepped appearance, suggesting at least two transverse fracture planes across different fiber bundles.
  - Frame 0: Small black spot just right of FOV center grows slightly between Frames 0 and 1. This point is clearly an earlier fracture location.
  - Frame 2: Black spot clearly grows, indicating a break in a bundle of fibers.
  - Frame 8: Fiber bundle involved in small black spot begins to clearly pull away leftward in FOV. Balance of strand still not clearly involved in failure.
  - Frame 16: Balance of strand begins to buckle, indicating transverse failure out of FOV left. Paint begins to be thrown vertically at point at top of strand just leftward of the small black spot; suggests failure is initiating on opposite face of the strand.
  - Frame 21: Transverse failure near grip severs remaining fibers. Gripward section will splinter all the way to the grip. Largest strand portion left of the fracture moves rightward in FOV, eventually striking grip metal portion and deflecting upward out of FOV by 1:23.
  - Portion already splintered at Frame 0 waves around but remains in frame for balance of video.
- B4-SP4_11855_Short.avi. Split portion visible, but relatively closely aligned with most of strand in beginning of this video. Focus not as sharp as 11853.
  - Frame 3: Areas of paint beginning to come off in discrete locations.
  - Frame 5: Paint appears to begin coming off across a large portion of the FOV, with a starburst region about 1 inch from the grip.
  - Frame 6: Disorganized starburst clearly evident.
  - Frame 9: Transverse failure across much of the strand evident at location of paint starburst. Segment attached to grip seen splintering and fraying.
  - Frame 11: By this frame, the leftward motion of the longer strand segment is apparent. The end is frayed, but most of that segment is intact compared to the piece attached to the grip. A fiber bundle, presumably the strands broken before the video cameras were started, can be seen intact.

- Batch 4 Specimen 4.xlsx shows a comparatively noisy load profile, with a number of small and one large unloading event after the two large grip-slips (grip seating events) at approximately 60 lbf.

S/N 8405/B4S5. HS 64k fps. Split failure mode: strand frayed and exhibited transverse splits before and during failure.

- B4-SP5-11853_short.avi.
    - Frame 0: Frayed fibers clearly evident. Light transverse line mid-strand at FOV left indicates a split.
    - Frame 2: Widening of strand, most intense just left of FOV center, indicates failure.
    - Frame 3: Failure clearly evident. Both segments pull away from fracture site. One fiber bundle stretches across the largest failure site. It will become clear that this bundle fails slightly leftward in Frame 4.
- B4-SP5-11855_short.avi.
    - Frame 0: A fiber or small bundle of fibers seen in motion between Frames 0 and 1. Frayed fibers evident.
    - Frame 2: Fibers expanding outward down much of strand center.
    - Frame 8: Main fiber bundle breaks at end of clear grip strain relief.
- Load profile Batch 4 Specimen 5.xlsx shows a number of small unloading events near time of failure.

S/N 8406/B4S6. HS, VIC trial. Center failure with pre-damage. VIC images are taken when strand load held constant. Failure occurred shortly after one of these load holds. VIC samples were all prepared with a coating of white paint speckled with black: these are the targets used to calculate strain in DIC.

- VIC3_11853_Short.avi.
    - Frame 5: Slight rightward motion of strand. Strand appears to begin to bulge.
    - Frame 6: Paint flakes and/or compression failure sites evident in many locations. Starburst beginning 1/5 of the way along length from grip. Leftward motion of bulk of strand away from this point.
    - Frame 7: Strand exterior fiber layer appears to be shattering, though some of this is likely paint.
    - Frame 12: Strand exhibits both lengthwise splitting and formation of short shards.
    - Frame 17: One long fiber bundle remains attached to grip.
- VIC3_11855_Short.avi.
    - Frame 4: Strand begins apparent expansion. Fiber bundle at top of strand and near grip begins to separate upward.
    - Frame 5: Failure point of separating strand appears to be about 1/3 of length from grip end of FOV.
    - Frame 7: Chaotic process well underway, with many transverse splits initiated in strand.
- IMG_5627.JPG shows long but thin fiber bundles remaining in grips.

S/N 8407/B4S7. HS 64k fps. Center failure with pre-damage.

- B4-SP7-11853_Short.avi.
  - Frame 4: Slight enlargement near grip.
  - Frame 5: Sharp transverse break at site of enlargement. Left segment accelerating leftward.
  - Frame 8: Segment ends split, frayed. Pronounced compression buckling at left end of left segment.
  - End of video: Short section of nearly intact strand segment remains in grip. Grip has moved rightward.
- B4-SP7-11855_Short.avi.
  - Frame 5: Clear motion of strand rightward toward grip to the extent that grip strain relief is beginning to deform.
  - Frame 6: Strand buckling in compression.
  - Frame 7: Buckle ~1 inch from grip failed, transverse fracture.
  - Frame 9: Left portion of strand continues travel toward grip, splintering itself and strand segment held in grip.
- Still photos include a number of shots of the fracture surfaces at various angles.
- Load profile shows significant decrease in load ramp rate with increasing load.

S/N 8409/B4S9. HS 64k fps. Center failure with pre-damage.

- B4-SP9_11853_Short.avi.
  - Frame 3: Movement in strand in out-of-focus left end of FOV, but none evident near grip.
  - Frame 4: Fiber bundle at image top of strand beginning expand outward and rightward toward grip.
  - Frame 5: Strand moving rightward.
  - Frame 6: Fiber bundle at image top of strand flexing in compression. Compression failure seen 2/3 of distance across FOV from grip end.
  - Several comparatively long strand segments remain at end of video.
- B4-SP9_11855_Short.avi.
  - Frame 3: Possible movement at left end of FOV.
  - Frame 4: Clear evidence of failure near to grip.
  - Frame 5: Compression failure initiating 3/4 way along FOV from grip.
  - Frame 9: Liberated segment has split into one large and several small fiber bundles, relatively intact along length. All move leftward toward grip seen in companion video view.
- Load profile shows significant decrease in load ramp rate with increasing load.

S/N 8410/B4-SP10. VIC. Center failure. From Fiber Break Status.pptx:

- A region of strain increase was observed approx. 20 lbf prior to failure. Comparison of still photo images before and after this region occurred shows a change in a particular location in the surface of the test article.

S/N 8408/B4-SP8. VIC. Cone disbond failure.

S/N 8513/B5SP13. HS. Cone disbond failure; invalid test.

- 5-SP13_11853_Short.avi.
  - Frame 6: Strand moving rightward toward grip. Grip strain relief begins to deform.
  - Frame ~19: Strand begins to buckle in compression.
  - By the end of the video, no strand break is evident.
- 5-SP13_11855_Short.avi.
  - Frame 5: Strand, including part of strain relief, is seen being pulled from grip.
  - Frame 16: Strand pulled out of grip.
- Load profile shows very significant decrease in load ramp rate with increasing load. Suggests that earlier instances of this anomaly are due to strand pulling partially from grip before failure.

S/N 8523/B5SP23. HS. Failure cause in gage section deemed likely secondary to a failure within the grip involving failure of the grip system itself. Peak load at failure among the lowest of these tested strands.

- B5-SP23_11853_Short.avi.
  - Frame 43: Strand with elastomeric bushing begins to be pulled from grip.
  - Frame 44: Strand begins apparent expansion.
  - Frame 47: Strand begins to split. One fiber bundle begins to buckle, and, in frame 48, fails.
  - Frame 57: Strain relief can be seen to be completely pulled free from grip. At 1:07, part of epoxy plug is seen pulling free, as well.
- B5-SP23_11855_Short.avi.
  - Frame 43: Strand seen moving rightward toward and into grip.
  - Frame 46: Separation and compression failure of a fiber bundle.
  - Frame 48: Buckling failure of same fiber bundle in a different location.
  - Frame 49: Buckling or compression failure of a number of fiber bundles close to grip, apparently a result of significant rebound.
- Load profile shows very significant decrease in load ramp rate with increasing load.
- IMG_6240.JPG shows strand failure that occurred inside the grip, as well as the white epoxy plug formerly attached to a cone-shaped section inside the grip.

S/N 8515/B5(4)S15. HS. Failed in longitudinal split.

- B5-SP15_11853_Short.avi.
  - Frame 11: Beginnings of strand expansion at left of FOV.
  - Frame 13: Clear evidence of a fiber bundle separating from main strand and buckling.
  - Frame 14: Fiber bundle fractured 3/4 of the way along FOV from grip. Second failure site begins to appear, giving rise to small compression event 1/4 of the way along FOV from grip, image bottom of strand.

  - Frame 15: Evidence of second failure site.
  - Frame 18: Transverse fracture site ~1/2 inch from grip. Strand pulls away, releasing many fiber bundles.
- B5-SP15_11855_Short.avi.
  - Frame 11-12: Strand expands. Small events occurring along strand.
  - Frame 12: Fiber bundle seen in companion video seen to buckle and kink ~1.5 inches from grip.
  - Frame 14: Fracture seen in fiber bundle.
  - Frame 18: Compression failure of main strand ~1.25 inches from grip.
  - By frame 55: Strand splits into multiple fiber bundles of various lengths.
- Still images, e.g. IMG_6257.JPG, show lengthwise splits in strand post-test.

S/N 8542/B5SP42. HS. Pre-damage. Failed in center.

- B5-SP42_11853_Short.avi. Strand shows significant stray fibers and/or small bundles at start of video.
  - Frame 9: Strand expands at left of FOV, but no movement seen near grip.
  - Frame 10: Motion communicated to grip end. Failure site appears to be out of FOV left.
  - By frame 33: Strand has disintegrated into short sections of fiber bundles.
- B5-SP42_11855_Short.avi. Heavy fraying at grip end.
  - Frame 1/2: Motion seen across FOV.
  - Frame 2: Compression failure apparent ~1.5 inches from grip.
  - Frame 5: Possibly distributed failure site, but significant failure occurring center of FOV.

S/N 8525/B5.3SP25. VIC. Sample painted white/ black speckles. Failed in the grip during a hold.

- B5.3-SP-25_11853_Short.avi.
  - Frame 10: Paint being thrown off at left of FOV. Strand moving to right: blurring of DIC speckles make this obvious.
  - Frame 12: Strand begins to buckle, but remains largely intact. Compression failure ~1.5 inches from grip.
  - Frame 13: Failure location evident at left edge of FOV. Strand begins to split into longitudinally split fragments. Most are large, but many are splintered through buckling.
  - By 2:00, many or most large splinters have Robin-Hooded into the grip elastomeric bushing.
- B5.3-SP-25_11855_Short.avi.
  - Frame 10: Paint seen thrown off at FOV right. Motion of strand toward grip becomes evident.
  - Frame 12: Compression failures seen near grip. Strand buckling.
  - Frame 13: Longitudinal fragments begin to be formed.

S/N 8514/B5.3S14. VIC. Sample painted white/ black speckles. Failed through a split with pre-damage.

- B5.3-SP14_11853_short.avi. Pre-damage clearly visible. Subtle motion seen in frayed fibers from beginning of video.
  - Frame 7: Significant apparent expansion of strand across FOV.
  - Frame 10: Strand seen disintegrating into fine slivers.
  - Frame 14: Significant area of transverse failure seen right at end of strain relief.
- B5.3-SP14_11855_short.avi.
  - Frame 7: Expansion at FOV left does not carry all the way to grip end of view.
  - Frame 8: Expansion seen to be longitudinal splits across FOV.
  - Frame 9: Large fiber bundle broken at strain relief. Strand beginning to splinter heavily.

S/N 8541/B5.3S41. HS, center failure with pre-damage.

- B5.3-SP41_11853_Short.avi. Pre-damage fraying clearly visible and in motion from beginning frame.
  - Frame 2: Strand clearly beginning to lose a bundle of fibers at FOV top edge of strand. Main part of strand deflecting slightly downward.
  - Frame 4: Failure at left end of FOV. Strand moving away from fracture and toward grip.
  - Frame 6: Compression failure near grip and near left end of FOV. Strand outer fibers coming off and turning into splinters.
  - Frame 16: Failure has produced a number of thick but short strand sections along with many small, thin splinters. Nearly all in this FOV are moving toward the grip.
- B5.3-SP41_11855_Short.avi. Pre-damage fraying actively moving.
  - Frame 4: Relatively clean single catastrophic fracture just right of mid-frame.
- Load trace Batch 5-3 SP41HS.xlsx shows clean break at peak load.

S/N 14/B5.5-SP14. VIC. Sample painted white/ black speckles. Center failure, but grip problem caused poor results. From B5.5-SP14_VIC3D.pptx:

- Several occurrences of strain localization were observed, but no definitive failure nucleation site was identified.
- Failure occurred in an area that did not show localized strain during a hold.

S/N 31/B5.7-SP31. VIC. Sample painted white/ black speckles. Did not fail: stopped pull test to examine splitting pre-damage more carefully.

S/N 17/B5.6-SP17. VIC. Sample painted white/ black speckles. Center failure, but grip problem caused poor results.

S/N 39/B5-6S39. Thermography. Grip disbond failure caused poor tensile test results.

- One large event before failure.
  - Comparison to load trace data was not attempted.

S/N 5/B5-6SP5. Thermography. Center failure, but grip problem caused poor tensile test results.

- Four large thermal events, including final failure event.
  - Two of the three pre-failure events may be visible in the load trace, but these two events are small in that graph.

S/N 27/B5-6SP27. Thermography. Grip disbond failure caused poor tensile test results.

- Two large and two small events.
  - Comparison to load trace data was not attempted.

S/N 8102/B2SP2. This strand was loaded to failure in tension before this study was performed. The remaining test article remnants were imaged using CT. Failure in the gage section was recorded.

- Observations from Video_1.mov:
  - Near one end of the imaged cross section of strand, there is a wedge of missing material associated with the strand fracture surface.
  - Most fibers are organized longitudinally, but some, particularly in the resin-rich area, meander considerably.
    - Even the longitudinally oriented strands were found after analysis to have measurable misalignment, some exceeding 5 degrees off longitudinal.
  - Longitudinal fractures are easily seen in the epoxy matrix.
    - In the fiber-dense region, the fractures meander in the transverse direction, but follow the strands longitudinally – they do not seem to cross strands often.
    - In the resin-rich region, the fractures meander both longitudinally and transversely.
    - Where the fractures transition between fiber-dense and resin-rich, there are artifacts in the image that look like strands following the fracture in the transverse direction. These are surmised to be structure in the fracture surface of the epoxy.
- From Video_2.mov:
  - The fracture surface exhibits a mixture of nearly intact, straight fiber regions; groups of fibers bent below the fracture surface, some to the extent of fracture; and fragmented fiber ends apparently still held loosely on the surface.
  - The longitudinal crack surfaces can be seen to include some broken fibers.
- The presentation *3D X-ray Microscopy of Single-Strand Tensile Test Specimen: Exploratory Data* and video fiber_breaks.mpg clearly show discontinuous fibers within the segment imaged.
  - Several images and some post-processing were required to be able to discern this.
  - It is not known how many of these fiber breaks were present in the strand before strength testing was performed. However, thermography suggests that at least some of these breaks could have occurred while the sample was under increasing load.

REPORT DOCUMENTATION PAGE	*Form Approved OMB No. 0704-0188*

1. REPORT DATE *(DD-MM-YYYY)*	**2. REPORT TYPE**	**3. DATES COVERED** *(From - To)*
01- 04 - 2016	Technical Memorandum	March 2013 - February 2016

4. TITLE AND SUBTITLE
Carbon Fiber Strand Tensile Failure Dynamic Event Characterization

5a. CONTRACT NUMBER

5b. GRANT NUMBER

5c. PROGRAM ELEMENT NUMBER

6. AUTHOR(S)
Johnson, Kenneth L.; Reeder, James

5d. PROJECT NUMBER

5e. TASK NUMBER

5f. WORK UNIT NUMBER
869021.05.07.05.23

7. PERFORMING ORGANIZATION NAME(S) AND ADDRESS(ES)
NASA Langley Research Center
Hampton, VA 23681-2199

8. PERFORMING ORGANIZATION REPORT NUMBER
L-20701 NESC-RP-13-00860

9. SPONSORING/MONITORING AGENCY NAME(S) AND ADDRESS(ES)
National Aeronautics and Space Administration
Washington, DC 20546-0001

10. SPONSOR/MONITOR'S ACRONYM(S)
NASA

11. SPONSOR/MONITOR'S REPORT NUMBER(S)
NASA/TM-2016-219188

12. DISTRIBUTION/AVAILABILITY STATEMENT
Unclassified - Unlimited
Subject Category 16 Space Transportation and Safety
Availability: NASA STI Program (757) 864-9658

13. SUPPLEMENTARY NOTES

14. ABSTRACT
Leads and members of the Composite Pressure Vessel Working Group (CPVWG) and of NASA Engineering and Safety Center (NESC) assessment TI-13-00912, Composite Overwrapped Pressure Vessel (COPV) Stress Rupture Reliability, requested visual and other primary engineering physics data regarding failure modes in carbon fiber strands relevant to composite pressure vessel reliability. This report contains the outcome of the NESC assessment.

15. SUBJECT TERMS
Composite Pressure Vessel Working Group; NASA Engineering and Safety Center; Composite Overwrapped Pressure Vessel; Stress Rupture; Tensile Failure; Carbon Fiber Strand

16. SECURITY CLASSIFICATION OF:			**17. LIMITATION OF ABSTRACT**	**18. NUMBER OF PAGES**	**19a. NAME OF RESPONSIBLE PERSON**
a. REPORT	**b. ABSTRACT**	**c. THIS PAGE**			STI Help Desk (email: help@sti.nasa.gov)
					19b. TELEPHONE NUMBER ***(Include area code)***
U	U	U	UU	45	(443) 757-5802

Standard Form 298 (Rev. 8-98)
Prescribed by ANSI Std. Z39.18